6818 *Macromolecules* **2010**, *43*, 6818–6828
DOI: 10.1021/ma101083a

Macromolecules
ARTICLE

Surface Behavior of PS_n(P2VP-*b*-P*t*BA)$_n$ Heteroarm Stars

I. Choi,[†] R. Gunawidjaja,[†] R. Suntivich,[†] C. Tsitsilianis,[‡] and V. V. Tsukruk*,[†]

[†]*School of Materials Science and Engineering, Georgia Institute of Technology, Atlanta, Georgia 30332-0245, and* [‡]*Department of Chemical Engineering, University of Patras, 26504 Patras and Institute of Chemical Engineering and High Temperature Processes (FORTH/ICE-HT), Greece*

Received May 15, 2010; Revised Manuscript Received July 2, 2010

ABSTRACT: We report the surface behavior and morphologies of two series of pH-responsive amphiphilic heteroarm star block copolymers. In this respect, we studied polystyrene/poly(2-vinylpyridine)/poly(*tert*-butylacrylate), PS_n(P2VP-P*t*BA)$_n$, heteroarm star block terpolymers and their precursors, PS_nP2VP$_n$, star copolymers. These star block polymers differ in architecture (copolymer vs terpolymer), block topology, arm length (molecular weight of P*t*BA segments varies from 8 900 up to 15 250 Da), and number of arms (n = 9, 22, and 28). The $\pi-A$ isotherms at different subphase pH (pH 5.8 and 2.0) exhibited strong pH dependence, leading to different limiting molecular area and surface micelle stability. Because of the pH-induced ionization of the P2VP block, the surface morphology of star copolymers bearing the free P2VP arms was strongly dependent on the pH of the subphase, whereas the star terpolymers containing the protonated hydrophilic P2VP block as midblocks maintained the same circular morphology at low pH and high pressures. The surface morphologies suggested that the high number of arms promoted the formation of unimolecular micelles, which are stable under varying deposition conditions.

Introduction

The supramolecular organization of macromolecules through self-assembly is considered to be an effective means for the control of physical and chemical properties of the organic ultrathin film at the interface.[1−3] The surface morphology, aggregate behavior, spatial order, and orientation of the microdomain of these ultrathin films (below 100 nm) are closely related to the microstructure of their polymeric building blocks.[4] The final organization of these ultrathin films depends on the chain architecture, shape, composition, nature of monomeric units, and intermolecular interaction of the polymer with itself or with the substrate. These factors play a critical role in the formation of well-defined structure with ordering on a nano- and microscale.[5−8]

Branched macromolecules have been widely used for studying ultrathin films because of their unique and diverse chain architectures as compared with their corresponding linear counterparts. Star-shaped polymers belong to the class of branched organic materials that includes dendrimers, hyperbranched, and dendronic molecules.[9] They have a molecular structure composed of a number of peripheral arms chemically bonded to a single core.[10−12] Recently, star-shaped block copolymers have gained considerable attention in terms of micelle aggregation and microphase separation in bulk, solution, and at the surface and interface as a result of their well-defined macromolecular architecture.[13−16] For example, heteroarm star copolymers, (also called miktoarm polymers) consist of an equal number of two different pure arms (A_nB_n).[17−21] The crowding of chains and multiple chain ends of these star copolymers account for their unique micellization behavior with diverse physical and chemical properties.[22−29]

The surface morphology of star block copolymers is controlled by a variety of factors such as the number of arms, degree of polymerization, composition, and chain architecture.[27−29] Accordingly, studies on their interfacial properties can offer more information on the structure−property relationship of ultrathin film formation. In the end, such an effort will lead to their potential applications in advanced functional systems such as ultrathin coatings, sensors, and drug carriers, for which responsive properties to external stimuli (e.g., pH, temperature, and shear) are required.[30]

Polystyrene/poly(2-vinylpyridine) (PS_nP2VP$_n$) heteroarm star copolymers synthesized via the "in−out method" with pH-sensitive ionizable P2VP segments showed associative properties in the solution state in the presence of toluene, which acts as a selective solvent. They were considered to be unimolecular micelles below the critical micelle concentration (cmc) and formed supermicelles above the cmc adopting a spherical shape with a core−shell structure.[20,22] When compared with corresponding linear counterparts, these heteroarm star copolymers showed three orders of magnitude higher cmc and an order of magnitude lower aggregation number. This was attributed to thermodynamically less favorable conditions to form micellar associates, as indicated by a positive Gibbs energy at higher temperatures. The effect of the length of insoluble arms in PS_nP2VP$_n$ heteroarm star polymers on their aggregation behavior in toluene was also considered.

The aggregation behavior of these amphiphilic PS_nP2VP$_n$ star polymers was also examined in acidic aqueous solution where the P2VP arms are protonated, exhibiting polyelectrolyte characteristics.[17,22] Single molecular conformations and dimensions of core−shell structure of unimolecular and multimolecular micelles of PS_7P2VP$_7$ stars were studied in various solvents, at different pH, and concentration conditions using atomic force microscopy (AFM) with improved contrast through metallization.[31,32] Yu et al. prepared an asymmetric amphiphilic PS-P2VP heteroam star copolymer via atom transfer radical polymerization (ATRP) and demonstrated the morphology change of polymolecular micelles of star polymer in a tetrahydrofuran and methanol mixed solvents.[33] The results revealed a change in morphology from irregular spherical and short rodlike aggregates (10% methanol) to rodlike micelles (90% methanol) by increasing the methanol concentration, which is a poor solvent for PS arms.

*Corresponding author. E-mail: vladimir@mse.gatech.edu.

 Published on Web 07/21/2010

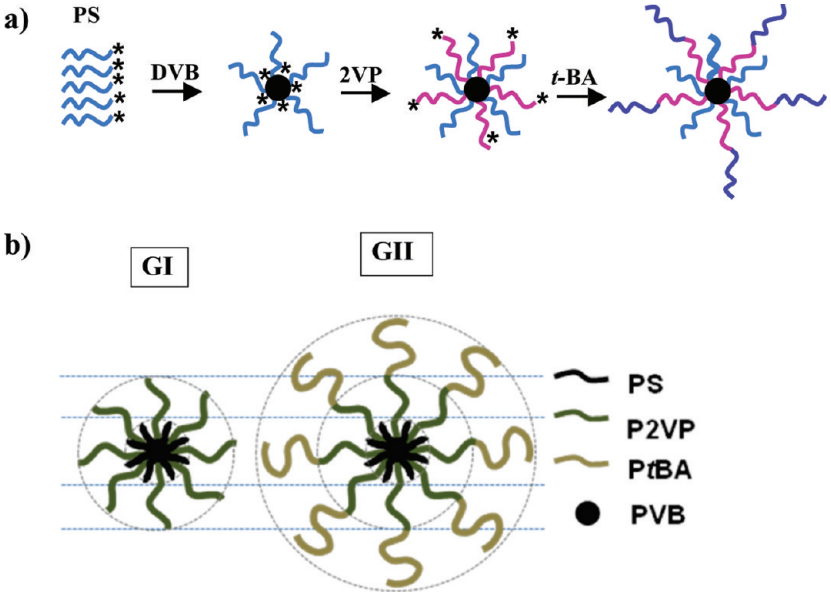

Figure 1. (a) Schematic of the multistep synthetic procedure for the synthesis of $A_n(B-C)_n$ heteroarm star block terpolymer; * denotes active sites. (b) Molecular structures of heteroarm star polymers. G I represents PS_nP2VP_n (A_nB_n) star copolymers and G II represents PS_n(P2VP-P*t*BA)$_n$ star block terpolymers.

The systematic study of quasi 2D surface micelles based on linear amphiphilic diblock copolymers was reported by Eisenberg et al.[34] Since then, the surface aggregation behavior of macromolecules has offered insight into the formation mechanism of ultrathin monolayers and their structural characteristics.[35−38] Various parameters such as aggregation number, geometric dimensions of surface micelles, and their shape have been explored through pressure−area isotherms and by transmission electron microscopy (TEM) and AFM of Langmuir−Blodgett (LB) monolayers. Final aggregation behavior depends on the composition, degree of polymerization, hydrophilic/hydrophobic balance, arm length, concentration of spreading solution, solvent polarity, and subphase pH and ionic strength. These surface micelles can be formed in solution, are compression induced, or can form spontaneously upon spreading at the air−water interface.[39] More recently, there have been reports on surface micelles, chain conformations, and morphologies of amphiphilic binary heteroam star copolymers having symmetric or asymmetric chain structure (e.g., polystyrene-*star*-poly(ethylene oxide), polystyrene-*star*-poly(2-vinyl pyridine), polystyrene-*star*-poly(acrylic acid), and poly(ethylene oxide)-*star*-poly(ε-caprolactone)).[40−42,26,29]

Recently, novel star-shaped $A_n(B-C)_n$ multisegmental block terpolymers bearing PS, P2VP, and PAA blocks were synthesized through an extended "in−out method" and were explored in aqueous media. These star terpolymers consist of pure PS arms and an equal number of P2VP-*b*-PAA diblock copolymer arms, PS_n(P2VP-*b*-PAA)$_n$, named heteroarm star block terpolymers. Hammond et al. demonstrated the hierarchical self-organization of such complex structures with small surfactants.[43] The ampholytic nature of this novel star block terpolymer allowed for complexation to be carried out on either the P2VP blocks (with negatively charged surfactants) or on the PAA blocks (with positively charged surfactants), depending on the pH at which the complexation reaction was carried out. The addition of surfactants to one block versus the other results in dramatically different morphologies, and when the P2VP blocks are complexed, close-packed spheres are observed. When the PAA blocks are complexed, the molecules form core−shell cylinders (PS and P2VP composing the core and shell, respectively) in a matrix of PAA.

However, studies of the surface micelles of $A_n(B-C)_n$ star terpolymers are still rare. Moreover, triblock ABC copolymers offer diverse morphologies with over 30 phases in the solution and bulk state because of the introduction of a third block. Such diverse morphologies cannot be observed in binary AB diblock or ABA triblock systems.[44,45] Therefore, it is intriguing whether these $A_n(B-C)_n$ star terpolymers can provide diverse surface supramolecular nanostructures with various core−shell-corona structures such as spherical, worm-like, vesicles, toroids, and Janus micelles, as observed with ABC linear counterparts.[46−51]

Here we explore the surface behavior and morphologies of a series of pH-responsive amphiphilic star block terpolymers, PS_n(P2VP-P*t*BA)$_n$, and their precursors, heteroarm star copolymers, PS_nP2VP_n, with a high asymmetry in arm length. The focus of this work is on the effect of pH on the morphology of these amphiphilic star-shaped multiblock polymers which differ in architecture (copolymers and terpolymers), arm/block length (molecular weight of P2VP segments), and number of arms (n = 9, 22, and 28). To investigate the molecular aggregation and microphase separation of complex amphiphiles at the air−water/air−solid interface, we focused on morphological studies at different subphase pH (pH 5.8 and 2.0). Our results demonstrate a strong pH dependence of the surface aggregation leading to different limiting molecular areas and resulting in distinct surface morphologies for stars with different chemical compositions.

Experimental Section

Materials. The PS_n(P2VP-P*t*BA)$_n$ heteroarm star block terpolymers were synthesized by a multistep, one-pot, sequential anionic living polymerization procedure following the "in−out method".[18,22] According to this routine, the first generation of PS arms was formed in the first step by reacting sBuLi with styrene (Figure 1a). These "living" linear PS chains were used in a subsequent step to initiate the polymerization of a given amount of divinylbenzene (DVB) acting as a cross-linking agent. A living PS star-shaped polymer was thus formed, bearing within its polyDVB core an equal number of active sites with its arms. In the third step, a second generation of arms was grown from the core upon the addition of 2VP. Part of the reaction medium was sampled out, and the PS_nP2VP_n precursor was isolated and characterized. In the remaining solution, the

Table 1. Molecular Characteristics of Heteroarm Star Polymers

		number of arms		A		B		C			
sample	chemical structures	N	total	M_w	N_{PS}	M_w	N_{P2VP}	M_w	N_{PtBA}	Φ_{P2VP}[a]	$M_{w,tot}$
GI-B9	PS_nP2VP_n	9	18	3400	33	13 200	126			0.80	149 000
GI-B22		22	44	3500	34	14 300	136			0.80	386 000
GI-B28		28	56	3000	29	16 000	152			0.84	529 000
GII-T9	PS_n(P2VP-PtBA)$_n$	9	18	3400	33	13 200	126	8900	69	0.52	235 000
GII-T22		22	44	3500	34	14 300	136	15 250	119	0.44	717 000
GII-T28		28	56	3000	29	16 000	152	11 000	86	0.53	843 000

[a] Weight fraction of P2VP.

sites located now at the ends of the second generation of P2VP arms are "living" and were used to polymerize the third monomer (t-BA), leading to PS_n(P2VP-PtBA)$_n$ heteroarm star block terpolymer. All samples have been characterized by a combination of gel permeation chromatography, ^{1}H NMR, and light scattering in accordance with the approach published elsewhere and summarized in Table 1.[43]

Substrate Preparation. Freshly cut silicon substrates with dimensions 1 × 2 cm^2 and [100] orientation (Semiconductor Processing) and a native silicon dioxide layer having a 1.6 nm thickness were cleaned with piranha solution (3:1 concentrated sulfuric acid and hydrogen peroxide mixture) in accordance with usual procedure.[52] Subsequently, it was abundantly rinsed with Nanopure water (18.2 MΩ cm) and dried with a dry nitrogen stream. Pretreated substrates served as a hydrophilic base for film deposition.

Fabrication and Characterization of Monolayers. The Langmuir−Blodgett (LB) studies were conducted using a KSV2000 minitrough at room temperature according to the usual procedure adapted in our lab.[53] A 0.50 to 0.10 mg/mL concentration of solution, composed of a star polymer sample dissolved in a nonselective solvent of chloroform/methanol mixture (90/10% in vol/vol) (HPLC grade), was prepared. The LB minitrough was next filled with Nanopure water. We adjusted the pH of the water subphase by using hydrochloric acid without a buffer. The 60−120 μL polymer solution was dispersed in several droplets evenly onto the surface of the water. It was then left for 30 min to allow for the evaporation of the chloroform. Compression of the monolayers was conducted at a speed of 5 mm/min. The Langmuir monolayers were transferred from the air−water interface by vertically pulling out the substrate submerged in the water subphase at a rate of 2 mm/min. The limiting cross sectional area A_0 was determined by the steepest tangent rise in the surface pressure, which evidenced the formation of a condensed monolayer.[54]

Effective monolayer thicknesses were obtained with a M-2000 U spectroscopic ellipsometer with WVASE32 analysis software. AFM images were obtained with a Dimension-3000 atomic force microscope. AFM images were generated in the "light" tapping mode with an amplitude ratio within 0.90 to 1.00 to avoid monolayer damage.[55] The AFM cantilevers had spring constants in the range of 40−60 N/m. Scanning rates were between 1.0 and 2.0 Hz, depending on the scan area that ranged from 40 × 40 to 0.5 × 0.5 μm^2.[56] Measurement of the contact angles was undertaken with a KSV CAM101 setup by dropping Nanopure water at three different locations for each sample.

Results and Discussion

Chemical Composition. Two groups of star polymers with different compositions, chain architectures, block topologies, and number of arms were used in this study. Group I includes heteroarm star copolymers composed of PS and P2VP arms (PS_nP2VP_n), where n denotes the number of each arm (Figure 1). Group II, represented as PS_n(P2VP-PtBA)$_n$, are star polymers composed of three kinds of blocks, which bear PtBA blocks as another hydrophobic component directly connected to the end of the P2VP arms. In both stars, the arms are linked on the same polydivinylbenzene (PDVB) core (Table 1 and Figure 1). Group I heteroarm star copolymers and Group II heteroarm star block terpolymers will be abbreviated as G I and G II, respectively, throughout this manuscript.

Figure 1b represents the general macromolecular architecture of the heteroarm star polymers studied here. For the sake of brevity, PS_nP2VP_n are termed as star copolymers and PS_n(P2VP-PtBA)$_n$ are termed as star terpolymers. The two groups have a different number of arms (n = 9, 22, and 28, respectively), and the total arm number is 18, 44, and 56 per single star polymer, respectively (Table 1). Φ_{P2VP} presents the weight percent of P2VP blocks indicating the hydrophilicity of the star polymers under the condition that pyridine groups in P2VP are ionizable. Overall, the star copolymers, PS_nP2VP_n (Φ_{P2VP} = 0.8), are more hydrophilic than the star terpolymers, PS_n(P2VP-BtBA)$_n$ (Φ_{P2VP} = 0.4 to 0.5).

On the basis of the ionization constant of pyridine (pK_a = 5.2) in solution, P2VP remains highly protonated under acidic conditions at pH 2.0 (adjusted by hydrochloric acid), whereas it is only partially ionized at pH 5.8 (Nanopure water without pH adjustment).[62] However, the effective pK_a value of the star polymer is expected to be lower (< 5.2) than the linear counterpart because of ionic confinement phenomena, which leads to high osmotic pressure within the star architecture.[57] Li et al. reported that PtBA homopolymer and PS-b-PtBA linear block colymer spread at the air−water interface, whereas PS homopolymer does not.[58] PtBA chain ends in star terpolymer thus seem to be surface-active and form surface aggregates. However, they are likely to be classified as hydrophobic on the basis of their hydrophilic/hydrophopobic balance.

Surface-Pressure Isotherms at Air−Water Surface. Figure 2 shows the pressure−area isotherms (π−A) of G I star copolymers and G II star terpolymers as a function of the number of arms and at different subphase pH. The initial molecular area, A_1, defined as the starting lift-up point of the surface pressure from zero pressure, depends on the number of arms (their molecular weight) under both pH conditions (Table 2). The π−A isotherm plots show a large range of high compressibility at the low-pressure region until they start to increase dramatically. This gradual build up in pressure is due to the higher occupancy required for a larger number of arms, which are initially stretched at the air−water interface but sink to the water subphase with modest lateral compression. The heteroarm star polymers studied here have very large initial area, A_1, in a gas state at which star polymers exist as unimers with little interaction between them, resembling their state in solution below the cmc. Cross-sectional areas of initial gas states depend on the number of arms and the subphase pH for both groups. In the condensed-state region, limiting molecular area, A_0, also shows similar change in terms of number of arms for both G I and G II groups (Table 2). We determined the limiting molecular areas of all

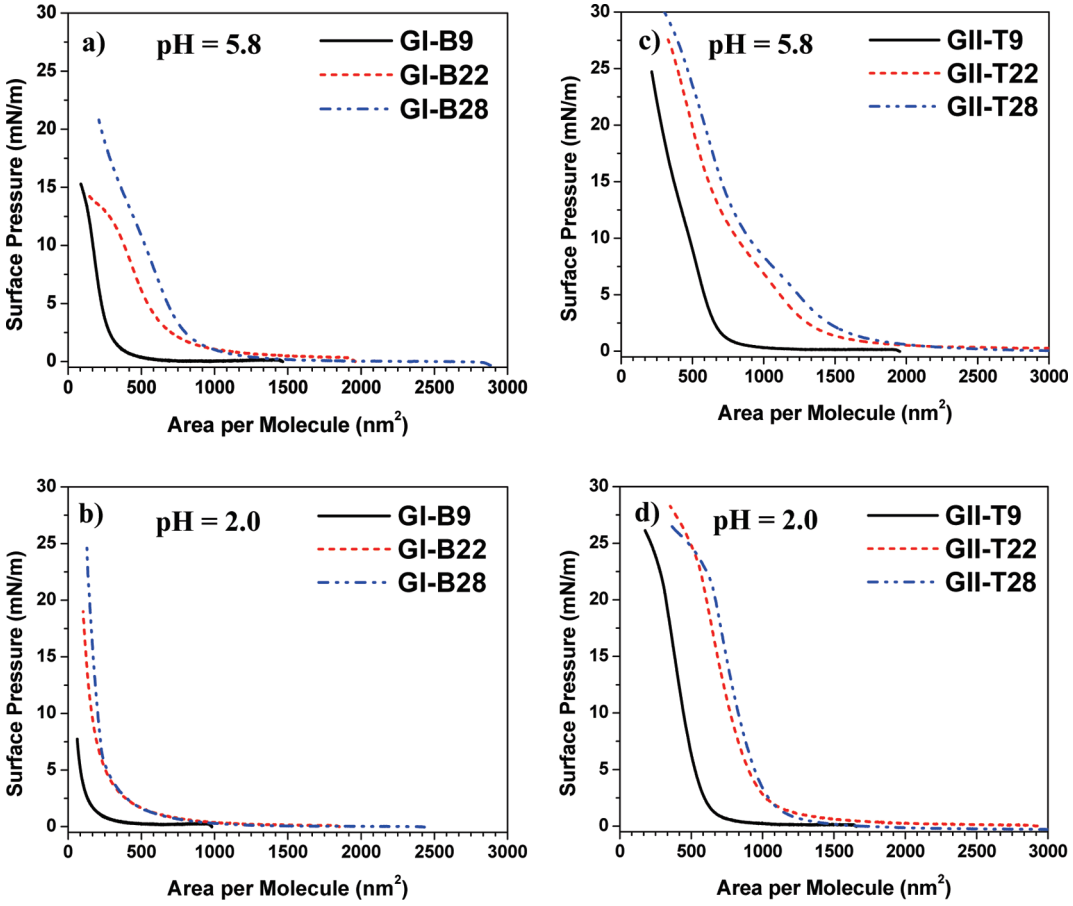

Figure 2. Pressure-area isotherms of (a,b) PS_nP2VP_n star copolymers and (c,d) $PS_n(P2VP\text{-}PtBA)_n$ star block terpolymers at different subphase pH (5.8 vs 2.0). GI-Bn denotes PS_nP2VP_n (n is the number of arms; n = 9, 22, and 28) and GII-Tn denotes $PS_n(P2VP\text{-}PtBA)_n$ (n = 9, 22, and 28).

Table 2. Monolayer Characteristics of Heteroarm Star Polymers at Different Subphase pH

	A_0, (nm²)		A_1, (nm²)		effective thickness (nm) P = 0.5 (mN/m)		P = 10.0 (mN/m)		P = 20.0 (mN/m)	
sample	pH 5.8	pH 2.0	pH 5.8	pH 2.0	pH 5.8	pH 2.0	pH 5.8	pH 2.0	pH 5.8	pH 2.0
GI-B9	340	120	1400	900	0.0	0.2	1.0	2.3	3.6	
GI-B22	750	260	1900	1800	0.6		1.4	3.0	4.1	
GI-B28	820	300	2800	2500	0.8	0.5	2.1	3.7	3.5	
GII-T9	750	580	1900	1800	0.4		1.1	1.1	2.0	
GII-T22	900	950	3400	2900	0.5		1.3	1.3	1.9	
GII-T28	1100	1100	3900	3400	0.6		1.6	1.3	1.9	2.0

star polymers by extrapolating the tangential line at the steepest rise to zero surface pressure in the range of surface pressures 5−20 mN/m.

The initial surface areas of compounds from the G II group are larger than those of G I compounds (Table 2). This effect could be attributed to the higher hydrophobic block content in the star terpolymers. Under acidic conditions, A_1 shows a smaller decrease as compared with that at neutral pH (Table 3). This difference can be caused by the fact that the ionized P2VP chain segments remain anchored to the air−water interface in a starfish shape with few submerged P2VP segments under these conditions. (See Figure 3 and more discussion below.)

G I and G II star polymers displayed distinct pH-sensitive surface pressure behavior. Under acidic pH (2.0) condition, the values of A_1 and A_0 decrease for G I, but stay constant for G II polymers. This distinct dependence on pH seems to be due to the difference in chain topology for these different groups. The relatively hydrophobic PtBA end blocks of G II

Table 3. Mophological Characteristics of Monolayers as a Function of Number of Arms under Different Subphase pH[a]

	average domain height (nm)		domain area coverage (%)		rms roughness	
sample	pH 5.8	pH 2.0	pH 5.8	pH 2.0	pH 5.8	pH 2.0
GI-B9	0.8	0.8	48.0	48.0	0.20	0.22
GI-B22	1.0	0.9	48.0	48.0	0.24	0.25
GI-B28	1.1	1.4	45.0	53.0	0.33	0.39
GII-T9	2.5	1.7	51.0	49.3	0.60	0.30
GII-T22	1.3	1.6	48.0	46.6	0.38	0.35
GII-T28	1.3	1.4	50.0	49.0	0.42	0.38

[a] Deposited at surface pressure 10.0 mN/m.

compounds influence the chain conformation change at the air−water interface, unlike G I compounds with pH-sensitive P2VP arms (Figure 1). In particular, we found that the shape of π−A isotherms under acidic pH conditions is similar to that for linear PS-P2VP block copolymers and PS-P2VP with incorporated alkyl groups.[36,62]

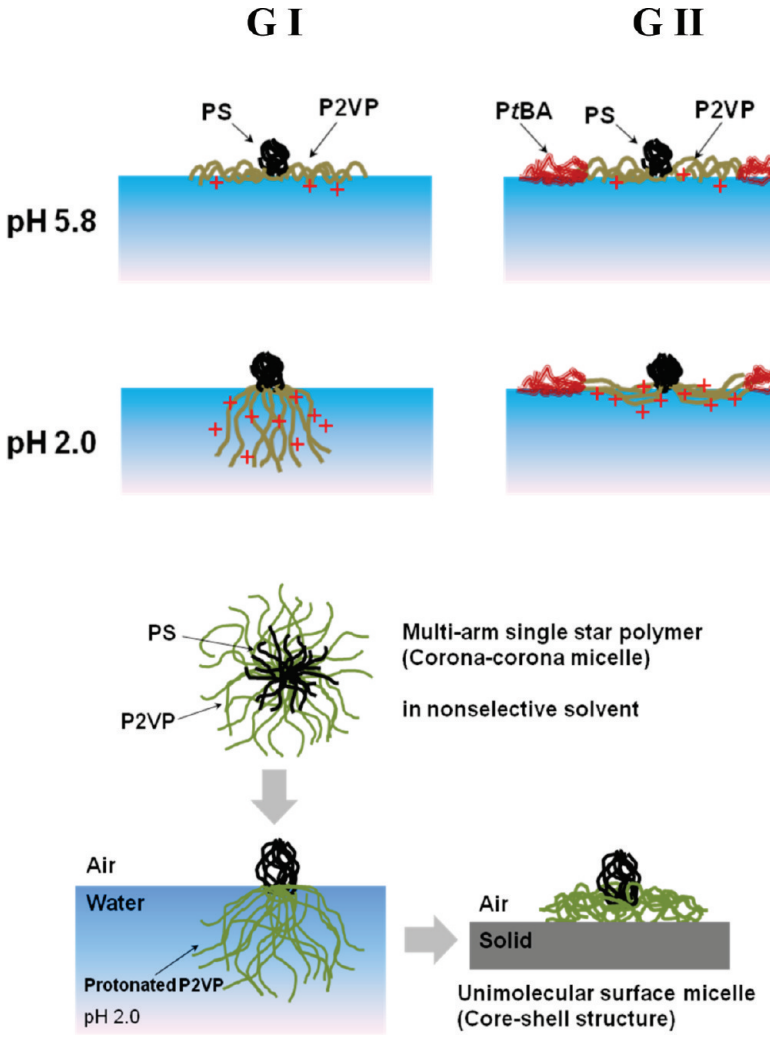

Figure 3. Schematics of suggested chain conformations of star copolymers (GI) (left) and star terpolymers (GII) (right) at pH 5.8 and 2.0 at the air−water interface under lateral compression (top) and unimolecular micelle at air−water and air−solid interfaces (bottom).

The pH dependence of surface isotherms reveals that G I compounds have notably smaller A_0 at neutral pH (pH 5.8) than under acidic pH (2.0) condition if compared with G II star terpolymers (Table 3). Under acidic pH, pyridine moieties (pK_a = 5.2) on P2VP blocks are ionized with a positive charge. The G I group shows a dramatic reduction in A_0 without any transition shoulder on the isotherms, whereas A_0 for G II compounds remains the same under the highly ionized condition (Figure 2). This behavior can be explained by the well-known characteristic transition model, that is, from "starfish" to "jellyfish" transition. (See Figure 3 and more discussion below.)[36,38] At higher surface pressure, the submersion of pyridinium chains into the water subphase occurs upon compression. Indeed, it has recently been found that the highly ionized P2VP arms of linear PS-P2VP diblocks might sink into the water subphase with increasing lateral compression depending upon the degree of ionization of pyridine groups without quaterization.[62] The hydrophobized version of PVP, alkylated PVP, remains adsorbed at the water surface without undergoing the conformation change and the chain submersion in the water subphase.[59]

However, the G II star terpolymers do not show any noticeable decrease in A_0 with pH change, contrary to the G I star copolymer precursors (Figure 2). $\pi-A$ isotherms of G II compounds show a weak transition shoulder in the range of 3 to 10 mN/m. At pH 2.0, the surface pressure undergoes a sharper transition in a solid state (Figure 2). However, A_0 of G II compounds remains the same under both pH conditions except for star polymers with a lower number of arms (GI-T9) (Table 2). This fact suggests that the P2VP-P*t*BA arms of G II star terpolymers reside in the adsorbed state on the water surface without a phase transition from the "starfish" to "jellyfish" conformation for both neutral and acidic pH (Figure 3). It is apparent that the hydrophobic P*t*BA chain ends, which are attached to P2VP arms, keep these diblock arms adsorbed onto the interface and not completely submerged in the water subphase. At pH 5.8, pyridine is partially protonated and remains adsorbed at the air−water interface because of the strong ionic repulsion, which causes the chain to be stretched along the interface. This intermolecular repulsion leads to a weak shoulder transition on the surface pressure isotherms for GII-T22 and GII-T28 at pH 5.8. At pH 2.0, the increased solubility of the fully protonated P2VP segments allows the chains to submerge easily into the water subphase (Figure 3). As a result, star molecules can be more highly compressed at pH 2.0 than at pH 5.8.

Compression−expansion isotherm cycles at different pH were conducted to measure the monolayer stability and the reversibility of surface aggregation (Figure 4). Langmuir monolayers were compressed up to 5.0 mN/m and subsequently expanded to 0.1 mN/m. The results show mostly

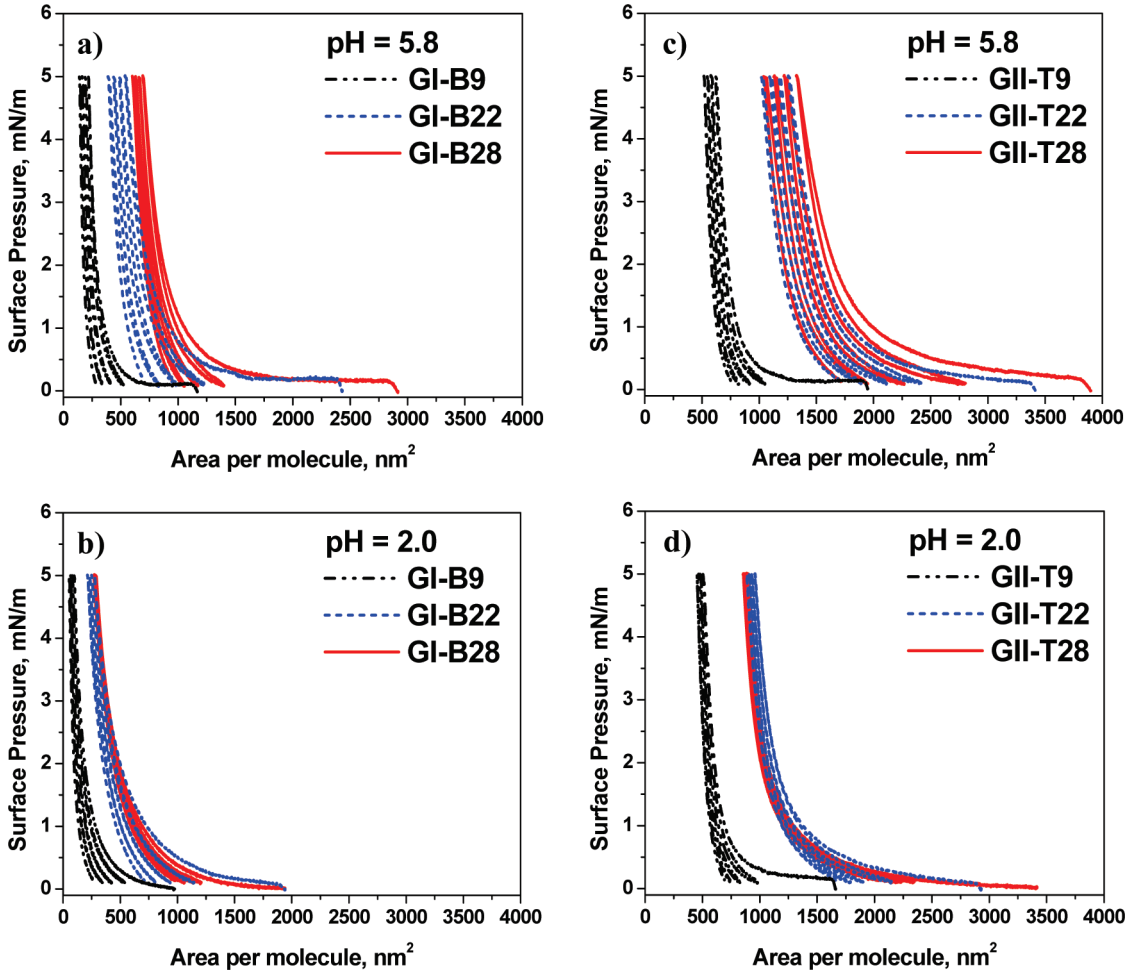

Figure 4. Compression−expansion cycles of (a,b) PS_nP2VP_n and (c,d) $PS_n(P2VP\text{-}PtBA)_n$ at different pH. The number of cycles is four.

reversible behavior of the compression−expansion cycle for G I and G II compounds under varying pH conditions in this compression range. Both G I and G II compounds exhibit higher hysteresis at pH 5.8 than at pH 2.0. G II compounds show a larger hysteresis, especially, at pH 5.8.

In addition, for both G I and G II groups, the hysteresis at pH 5.8 increases with the number of arms, whereas at pH 2.0, this trend does not depend on the number of arms within the same group. In the case of pH 5.8, higher hysteresis implies loose initial packing at the air−water interface, which can be ascribed to higher electrostatic repulsion between surface aggregates. We suggest that partially ionized P2VP segments, which are absorbed at the air−water interface, become reorganized, resulting in the transformation into a different chain conformation (Figure 3). This different conformation at pH 5.0 can be explained by the varying charge distribution on the partially ionized P2VP segments serving as a kinetic barrier.[38,60] The hydrophobic P*t*BA end blocks anchored to the surface act as additional elastic barrier, thereby preventing the close packing of the molecules. P*t*BA segments seem to sustain the ionized P2VP chains floating at the air−water interface by hindering the submersion of the P2VP block into the water subphase.

Limiting molecular area, A_0, varies linearly with the number of arms and the number of pyridine monomer units, although this conclusion is made with a limited number of data points (Figure 5). Extrapolating the limiting molecular area to zero content of P2VP monomer characterizes the micelle structure based on the contribution of each block to the surface area at the air−water interface. Previous reports on the limiting molecular area of surface micelles composed of linear block copolymers under neutral pH conditions showed a zero intercept.[61,62] However, a nonzero intercept observed in this study indicates that the PS cores contribute to the surface area at the air−water interface under low pH condition (15 nm^2 at pH 1.8).[62] G I group with free hydrophilic P2VP arms showed a lower intercept than G II group with two hydrophobic segments, PS and P*t*BA. It indicates that in the case of G I compounds, PS arms and P2VP arms remaining at the air−water interface account for the nonzero intercept. The relatively higher intercept for G II compounds is due to the contribution of additional long P*t*BA end blocks to the limiting molecular area. The higher intercept of these compounds at pH 5.8 than at pH 2.0 indicates that PS and P2VP arms of star polymer micelles contribute to their surface area, implying incompletely segregated chain-like structures at the air−water interface. The slope of the plots represents the area of each arm or the 2VP monomer unit at the air−water interface. G I shows a change in area of 2VP monomer unit from 0.16 nm^2 at pH 5.8 to 0.06 nm^2 at pH 2.0, whereas the slope for G II is similar under different pH conditions (0.11 nm^2 at pH 5.8 and 0.17 nm^2 at pH 2.0). These results reflect that the chain conformation of P2VP phase in G1 is more sensitive to pH than G II.

Figure 5c shows a linear variation of the number of arms with limiting molecular area under log−log scale, suggesting the power law dependence of the variables, $A_0 \approx n^{\alpha}$ in the range of parameters studied here. Therefore, we can

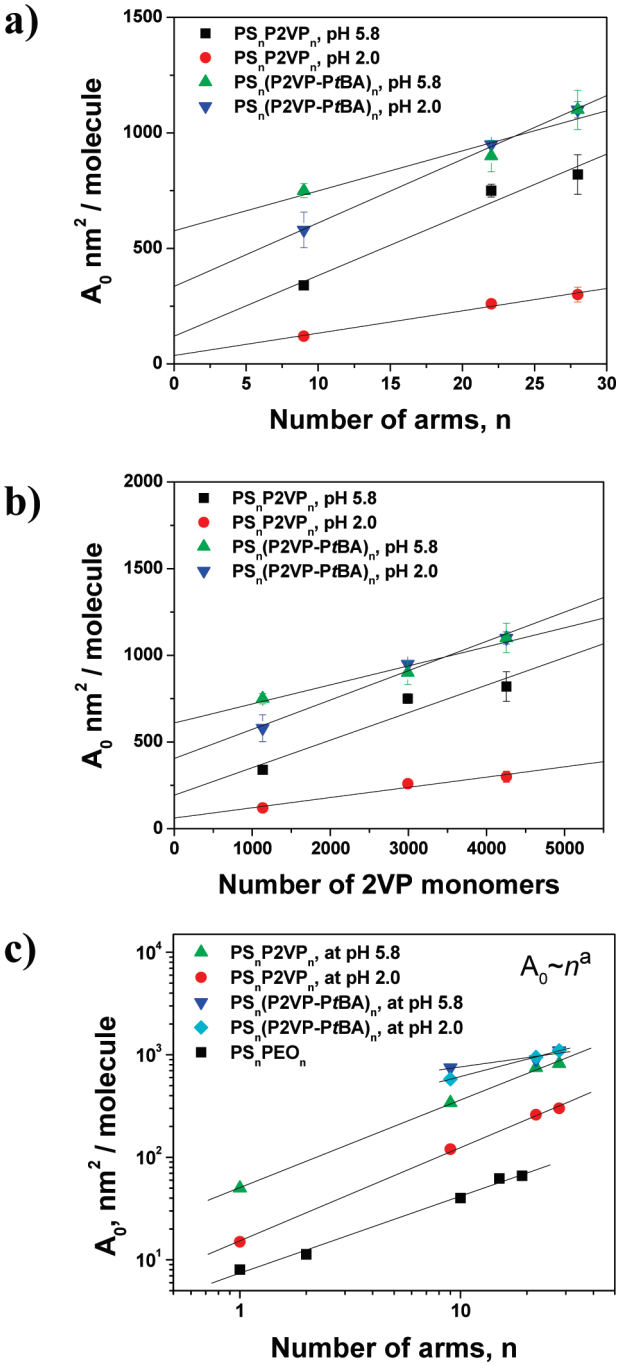

Figure 5. (a) Plot of limiting molecular area, A_0, of star polymers versus number of arms at different subphase pH 5.8 and 2.0 (PS_nP2VP_n at pH 5.8 (■) and 2.0 (●); PS_n(P2VP-P*t*BA)$_n$ at pH 5.8 (▲) and 2.0 (▼)). (b) Limiting molecular area, A_0, of star polymers versus number of 2VP monomer units at different subphase pH 5.8 and 2.0 (PS_nP2VP_n at pH 5.8 (■) and 2.0 (●); PS_n(P2VP-P*t*BA)$_n$ at pH 5.8 (▲) and 2.0 (▼)). (c) Limiting molecular area A_0 as a function of number of arms n for PS_nP2VP_n at pH 5.8 (▲), PS_nP2VP_n at pH 2 (●), and PS_n(P2VP-P*t*BA)$_n$ at pH 5.8 (▼) and 2.0 (◆) in comparison with star polymers PS_nPEO_n (■) from ref 28 and PS_2−PEO_2 from ref 26c. For n = 1, the data for corresponding diblock copolymer of PS-P2VP was taken from ref 62.

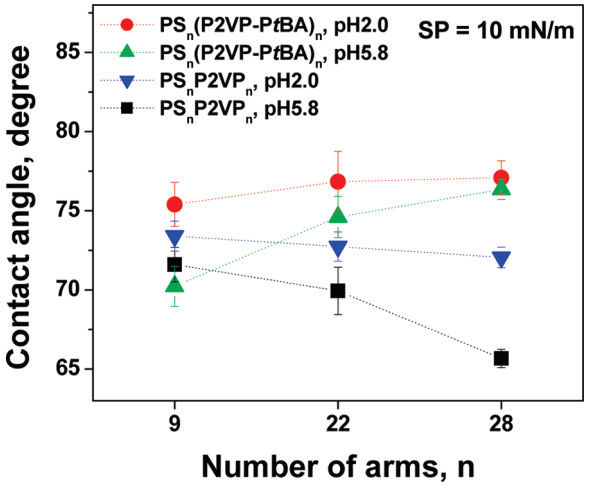

Figure 6. Contact angles measurements of Langmuir−Blodgett monolayers of star polymers. G II star terpolymers at pH 2.0 (●) and pH 5.8 (▲); G I star copolymers at pH 2.0 (▼) and pH 5.8 (■).

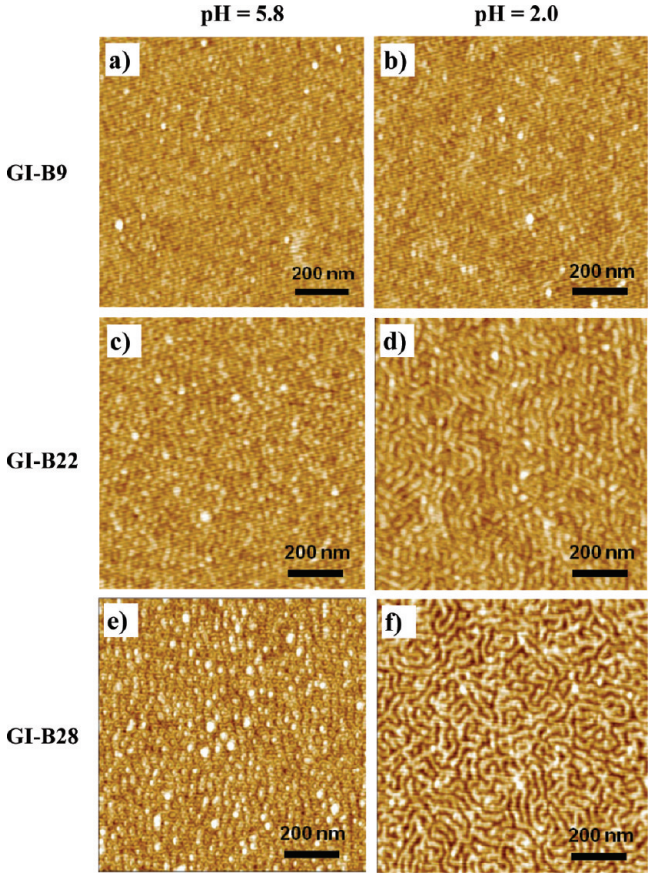

Figure 7. AFM topographical images (1 × 1 μm^2) of PS_nP2VP_n star copolymers (n = (a,b) 9, (c,d) 22, (e,f) 28) at different subphase pH: (a,c,e) pH 5.8 and (b,d,f) pH 2.0. The LB films were deposited at a surface pressure of 10 mN/m. GI-Bn denotes PS_nP2VP_n (number of arms, n = 9, 22, and 28). Z scale = 5 nm.

speculate that this dependence suggests that the surface aggregation behavior of our star polymer at the interface is analogous to the aggregation number dependency on the degree of polymerization of the different block copolymers in a solution state.[63] The analysis shows that the α value for the G I group is within 0.85 to 0.90 but decreases to 0.30 to 0.56 for G II group. These values can be compared with data for PS-PEO star block copolymer from our previous studies with exponential value α = 0.75 (Figure 5c). Larger α value implies there is a higher contribution of each arm to molecular area at the air−water interface. From comparison with surface behavior of a linear counterpart, we suggest that star architectures hinder the rearrangement of arms at the interface because they have the restriction of chain conformation

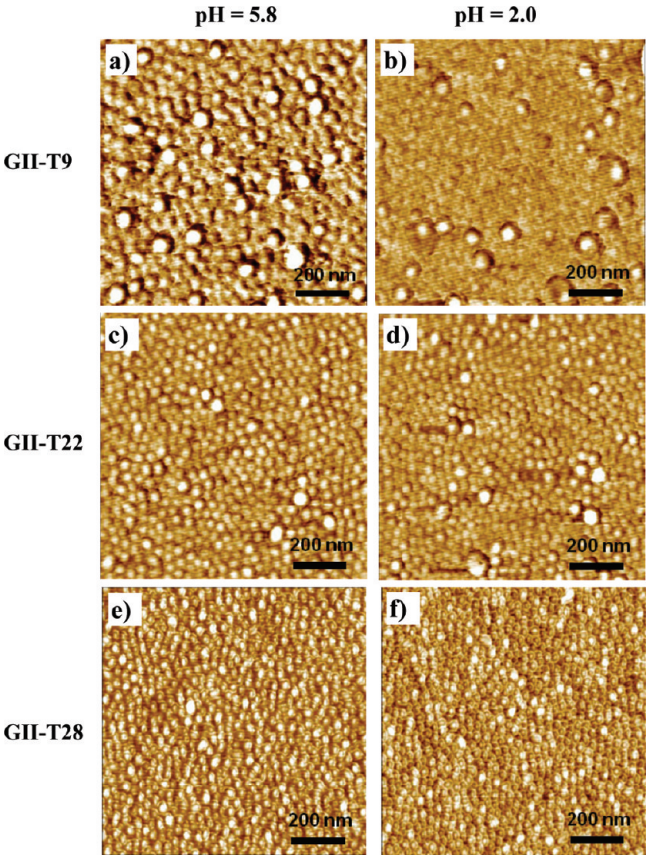

Figure 8. AFM topographical images ($1 \times 1\ \mu m^2$) of PS_n(P2VP-P*t*BA)$_n$ star block terpolymers (n = (a,b) 9, (c,d) 22, and (e,f) 28) at different subphase pH: (a,c,e) pH 5.8 and (b,d,f) pH 2.0. The LB films were deposited at a surface pressure of 10 mN/m. GII-Tn denotes PS_n(P2VP-P*t*BA)$_n$ (n = 9, 22, and 28). Z scale = 5 nm.

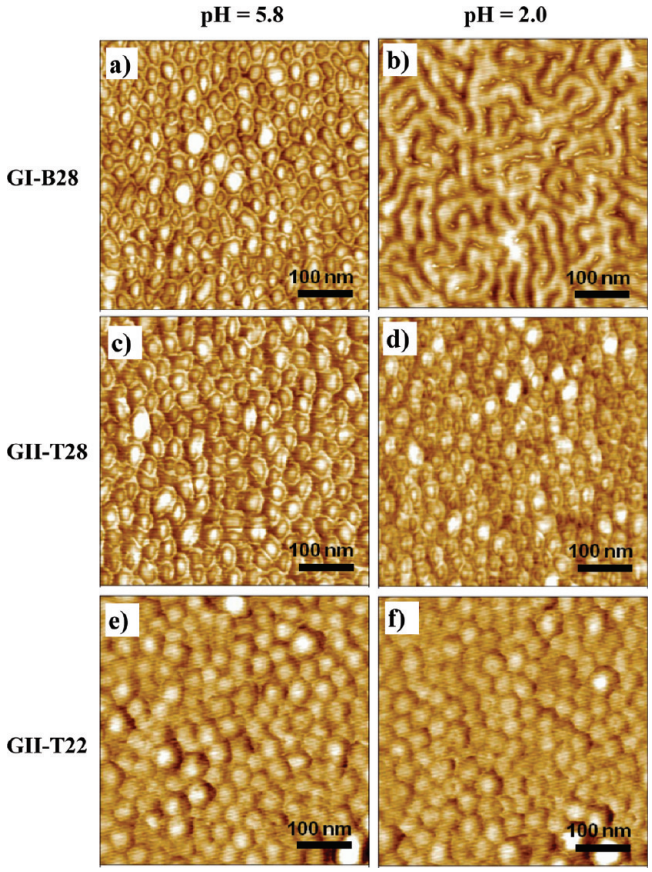

Figure 9. AFM topographical images ($500 \times 500\ nm^2$) of GI-B28 ((a,b) $PS_{28}P2VP_{28}$ star copolymers), GII-T28 ((b,c) PS_{28}(P2VP-P*t*BA)$_{28}$ star block terpolymers), and GII-T22 ((e,f) PS_{22}(P2VP-P*t*BA)$_{22}$ star block terpolymers. The LB films were deposited at surface pressure 10 mN/m at different subphase (a,c,e) pH 5.8 and (b,d,f) pH 2.0. Z scale = 5 nm.

due to confined and highly crowded chain structure around the core. A significant drop of α for G II group can be related to already high initial molecular area caused by the contribution from additional hydrophobic ends.

Monolayers at Solid Substrates. The effective thickness of Langmuir monolayers deposited at the surface pressure of 10 mN/m increases with the number of arms for both G I and G II groups (Table 2). At varying surface pressure, the effective monolayer thickness increases with increasing compression for the same number of arms. G I heteroarm star copolymers exhibit pH-dependent behavior of thicknesses (Table 2). Under acidic pH (2.0) condition, the effective thickness is three times higher than that at neutral pH. This result supports the suggestion made above that pressure induces chain reorientation in the vertical direction, which contributes to the monolayer thickness (Figure 3). The drastic increase in thickness under acidic conditions can be attributed to the swelling of the P2VP chain segment under acidic conditions due to intramolecular ionic repulsion, which leads to the expanded chain conformation. Moreover, the lateral compression provides smaller surface area per molecule, thus forcing the ionized P2VP chains to stretch further in a vertical direction.

In contrast, the effective thickness of the LB monolayer for G II star terpolymers undergoes no pronounced changes under different pH (Tables 2 and 3). Moreover, they exhibited similar thicknesses with group G I star copolymers despite much longer arm lengths. We suggest that hydrophobic block, P*t*BA, at chain ends plays a critical role in the stabilization of the lateral organization and the prevention of their starfish conformation even under acidic pH conditions (Figure 3). This behavior underlines the critical role of the nature of the end groups in the overall conformation of the star molecules at interfaces and their behavior under different pH conditions.

For LB monolayers formed with both groups of star polymers, the contact angle was within 65−77° (Figure 6), indicating the modestly hydrophobic composition of the topmost surface layer and confirming the preferential surface location of PS and PtBA blocks in accordance with models discussed above (Figure 3). A higher contact angle was observed for LB monolayers deposited under acidic conditions (Figure 6). The increasing contact angles under acidic pH suggest that the ionized P2VP blocks stretch out beneath the topmost PS phase, resulting in the enhanced vertical chain segregation of hydrophobic PS and hydrophilic P2VP blocks. The presence of the additional PtBA blocks in the G II star terpolymers results in a slightly higher contact angle (Figure 6). The contact angle of G I star polymers increases with the number of arms, in contrast with the G II group, which can be related to different surface morphologies and microroughness, as will be discussed in the next section (Table 3).

Surface Morphology of Monolayers. Figure 7 shows the surface morphology of LB monolayers of G I star polymers formed at different pH and at a surface pressure of 10 mN/m. The surface morphology changes from regular circular micelles at pH 5.8 to ribbon-shaped aggregates at pH 2.0. For a higher number of arms (GI-B22), a distinct labyrinth pattern was observed instead of a long ribbon or rod structure, as

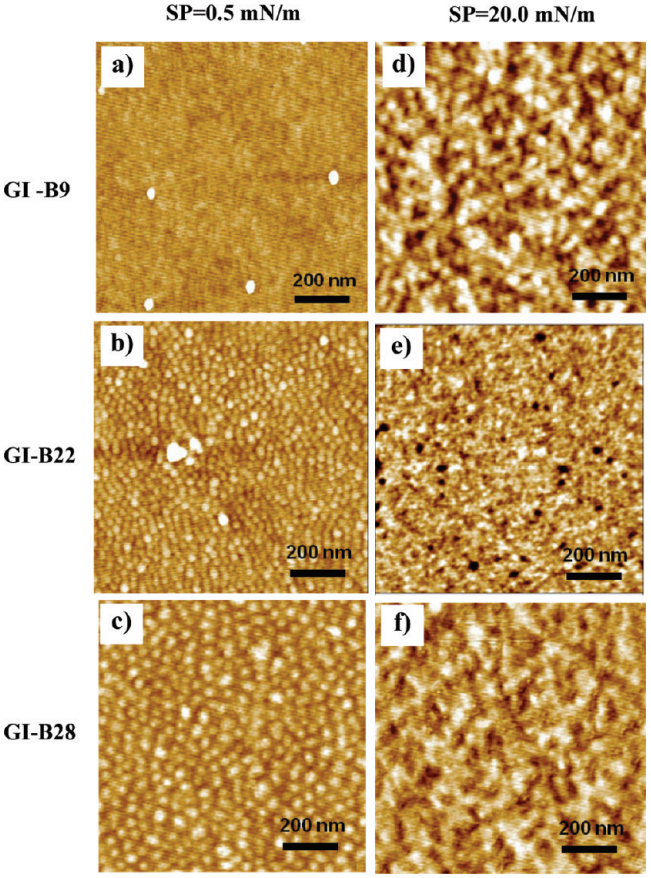

Figure 10. AFM topographical images (1 × 1 μm^2) of PS_nP2VP_n at different surface pressures (0.5 and 20.0 mN/m) at pH 5.8. GI-Bn denotes PS_nP2VP_n (n = 9, 22, and 28). Z scale = 5 nm.

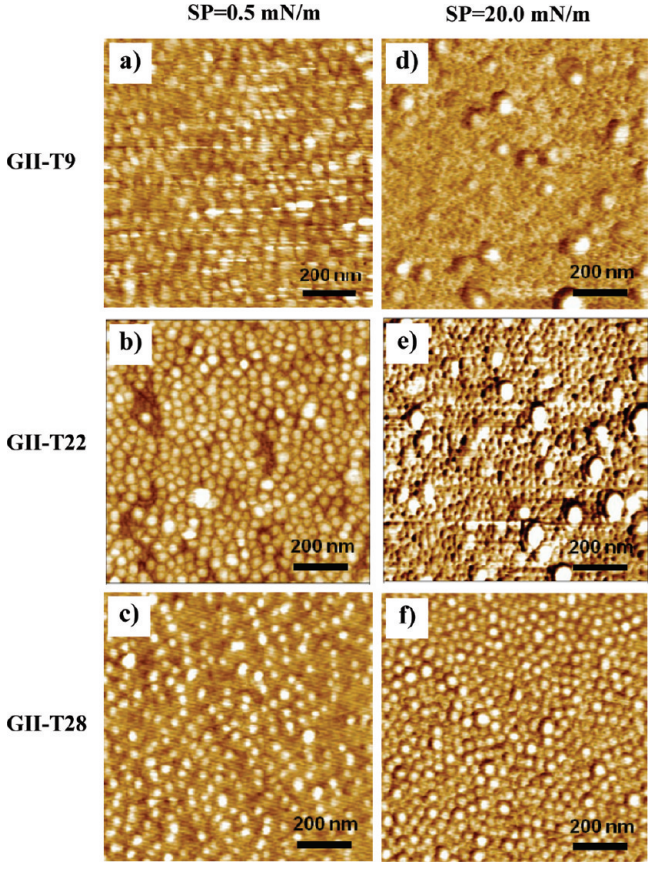

Figure 11. AFM topographical images (1 × 1 μm^2) of PS_n(P2VP-PtBA)$_n$ at different surface pressures (0.5 and 20.0 mN/m) at pH 5.8. GII-Tn denotes PS_n(P2VP-P*t*BA)$_n$ (n = 9, 22, and 28). Z scale = 5 nm.

previously reported for star block copolymers.[37,38] The circular micelles of PS-P2VP can be compressed up to high surface pressure and tend to form a labyrinth pattern caused by the fusing of PS cores into short rods.[60] This transformation provides further evidence of the submersion of ionized P2VP blocks (transition from starfish to jellyfish) at the air−water interface (Figure 3). It is noteworthy that at pH 2.0 the labyrinth pattern becomes more prominent with an increase in the number of arms. In the case of GI-B28, the surface aggregates are more curved and branched as compared with GI-B9 and GI-B22. However, at this pressure, intermicellar distance remains similar for many star polymers regardless of pH conditions.

In contrast, the G II star terpolymers show no significant pH-dependent transformations of surface morphology (Figure 8). The well-defined circular surface micelles with large diameters were maintained regardless of the variation of arm number with little change in the surface texture. However, GII-T9 exhibited smoother surfaces at acidic pH. The hydrophobic P*t*BA blocks appear to keep the ionized P2VP blocks floating, even at acidic pH, thereby suppressing the transformation of the molecular state from starfish into jellyfish (Figure 3).

In contrast with the G I group, whose micelle size increases with the number of arms for different pH, the size of micelles of the G II group decreases with increasing number of arms, as can be seen in high-resolution AFM images in Figure 9. For instance, GII-T9 compound with a smaller number of arms shows larger and more irregular micelles with an average diameter of 55 ± 5 nm. Diameters of domains for GII-T22 are slightly lower (45 ± 5 nm), and there is an even further decrease for GII-T28 to 38 ± 5 nm. Such shrinking can be caused by the coaggregation of PS and P*t*BA hydrophobic blocks in more crowded stars, resulting in a more condensed state.

Next, to elucidate the pH effect on the surface morphology and its transformations, the LB monolayers were compared at different surface pressures, particularly at 0.5 and 20.0 mN/m at neutral pH, as illustrated in Figures 10 and 11. At the low surface pressure of 0.5 mN/m, a more loose packing of circular surface aggregates is observed for both G I and G II groups. For compounds with the lowest number of arms, such as GI-B9, no clear micellar structures are observed. Moreover, increasing the number of arms effectively makes the micelle aggregates more defined and more separated. In particular, the G II-T28 compound shows a large uniform space between surface micelles.

At the higher surface pressure of 20 mN/m, the G I group shows coarse texture and collapsed monolayers contrary to the transformation from circular to lamellar morphology under acidic pH (Figure 7). However, G II compounds maintain the circular micellar structures at higher pressure and neutral pH, showing higher stability without collapsing, as displayed in Figure 11d−f. In particular, G II-T28, with a larger number of arms, exhibits a higher stability compared with compounds with a lower number of arms (GII-T9 and GII-T22). This observation confirms conclusions made on the basis of $\pi-A$ isotherm analysis and suggests that the hydrophobic P*t*BA corona serves as a more effective barrier under higher lateral compression than the hydrophilic corona of G I compounds, thus effectively preventing collapse of the circular micellar morphology.

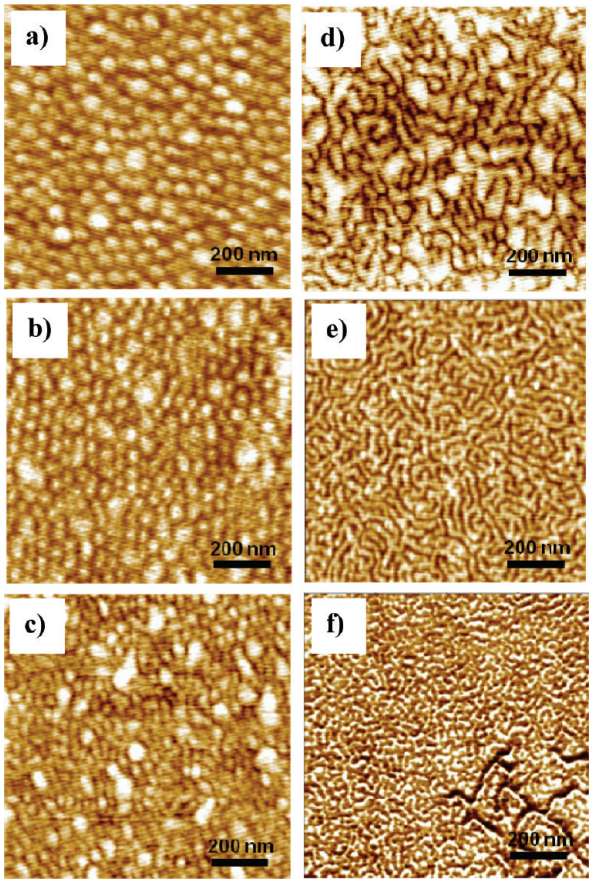

Figure 12. AFM topographical images ($1 \times 1\ \mu m^2$) of $PS_{28}P2VP_{28}$ star copolymer as a function of surface pressure: (a) 0.5, (b) 1.0, (c) 5.0, (d) 8.0, (e) 10.0, and (f) 30.0 mN/m at pH 2.0. *Z* scale = 5 nm.

To consider the formation of the labyrinth morphology under acidic pH (2.0) condition, we examined LB films at different surface pressures (0.5, 1.0, 5.0, 8.0, 10.0, and 30.0 mN/m) for selected compounds. We selected star polymers with the largest number of arms from G I group (GI-B28, $n = 28$) and from Group II (GII-T28, $n = 28$) (Figures 12 and 13). AFM imaging demonstrates that the labyrinth morphology has indeed originated from the transition from the initial circular structures observed at very low surface pressure (Figure 12a). As the lateral compression increased (1.0−5.0 mN/m), the surface morphology began a gradual transformation with compressed and coalesced circular domains (Figure 12b,c). At the intermediate state, a mixture of condensed circular and short ribbon is observed (Figure 12d). When compressed further to 10.0 mN/m, the surface morphology finally converts to fine, interwoven ribbon structures constituting the labyrinth morphology (Figure 12e). This morphology remains stable, although with much finer elements, up to the highest pressure (30.0 mN/m), close to the monolayer collapse. Therefore, the G I compound could readily undergo the conformation transformation from flattened arms (starfish) at the air−water surface into submerged P2VP blocks (jellyfish) under high surface pressure, leading to the easier collapse of these monolayers (Figure 3).

In contrast with the $PS_{28}P2VP_{28}$ compound discussed above, no significant changes in the morphology were observed for the G II star terpolymers with an identical number of arms under the same pH conditions (Figure 13). PS_{28}-(P2VP-P*t*BA)$_{28}$ sustains the stable circular structures, confirming that the hydrophobic P*t*BA end blocks prevent the aggregation/transformation by acting as natural barriers that

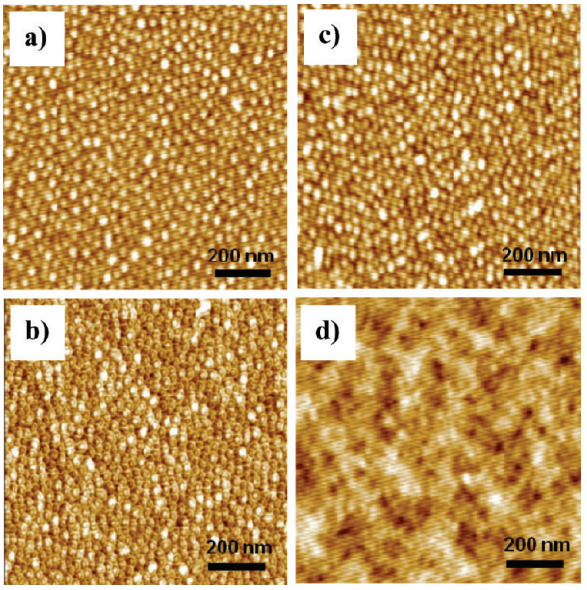

Figure 13. AFM topographical images ($1 \times 1\ \mu m^2$) of PS_{28}(P2VP-P*t*BA)$_{28}$ as a function of surface pressure: (a) 1.0, (b) 10.0, (c) 25.0, and (d) 30.0 mN/m at pH 2.0. *Z* scale = 5 nm.

Table 4. Aggregation Numbers of Surface Micelles

sample	pH	SP (mN/m)[a]	A_{mol} (nm^2/molecule)[b]	N_{micel} (n)[c]	A_{micel} (nm^2/micelle)[d]	N_{agg} (n)[e]
GI-B28	5.8	0.1	1723	21 ± 2	2976 ± 0.5	1.7 ± 0.5
	5.8	10.0	520	74 ± 4	845 ± 0.3	1.6 ± 0.3
GII-T28	5.8	10.0	897	48 ± 5	1302 ± 0.2	1.5 ± 1.0
	2.0	10.0	829	60 ± 7	1042 ± 0.4	1.3 ± 0.8

[a] Surface pressure. [b] Molecular area from surface-area isotherms. [c] Number of micelle estimated from AFM images (250 × 250 nm^2). [d] Micelle area. [e] Aggregation number.

can endure the compression forces such as those suggested above (Figure 3). Finally, the monolayer collapse resulted in disorganized local regions of coalesced domains without any signs of labyrinth morphology (Figure 13d).

To characterize quantitatively the domain morphology for the star polymers with the largest number of arms (28), we derived the aggregation number (N_{agg}) from AFM images according to the known procedure.[34] The number of aggregates per selected surface area (A_{micel}) was compared with the molecular area (A_{mol}) from the limiting cross-section area, A_0, to derive N_{agg} (Table 4). Remarkably, it is found that the star polymers with a larger number of arms possess a very low aggregation number, around 1.5, at different pressures and pH. This fact indicates that domain structures in these star block copolymers are predominantly unimolecular micelles. This conclusion is in agreement with the models suggested above (Figure 3). Apparently, the overcrowding of the outer shell of the star molecules with a large number of long arms causes intramolecular aggregation and microphase separation and prevents the aggregation of multiple molecules into a single micelle. The formation of stable unimolecular aggregates is in contrast with regular, compositionally similar linear block copolymers, which show a large aggregation number.[22]

Conclusions

In this study, we reported the surface behavior and morphologies of two series of novel pH-responsive amphiphilic heteroarm star polymers, PS_n(P2VP-P*t*BA)$_n$ and PS_nP2VP_n, which differ in architecture, block topology, arm lengths (molecular weight of P*t*BA segments varies from 8 900 to 15 250 Da), and number of

arms (n = 9, 22, and 28). The $\pi-A$ isotherms of Langmuir monolayers at different subphase pH (pH 5.8 and 2.0) exhibited strong pH dependence, leading to the different limiting molecular area and surface micelle stability. Because of the pH-sensitive ionization of P2VP block, the morphology of star copolymers bearing the free P2VP arms was strongly dependent on the pH of the subphase, whereas the star terpolymer containing the protonated hydrophilic P2VP block as midblocks and terminal hydrophobic P*t*BA blocks maintained nearly constant organization at low pH.

The surface morphology studies suggested that star copolymers without end blocks can form circular micelles with larger sizes, which can be readily transformed to labyrinth morphologies with dense interpenetrating structures by compression and pH variation. The high number of arms and the presence of the hydrophobic end blocks of star polymers promote the formation of robust and stable unimolecular condensed micelles under different compressions and pH conditions.

Acknowledgment. This work is supported by National Science Foundation (NSF-DMR grant 0756273 and DMR-1002810).

References and Notes

(1) Tsukruk, V. V. *Prog. Polym. Sci.* **1997**, *22*, 247.
(2) Granik, S.; Kumar, S. K.; Amis, E. J.; Antonietti, M.; Balazs, A. C.; Chakraborty, A. K.; Grest, G. S.; Hawker, C.; Janmey, P.; Kramer, E. J.; Nuzzo, R.; Russell, T. P.; Safinya, C. R. *J. Polym. Sci., Part B: Polym. Phys.* **2003**, *41*, 2755.
(3) Forster, S.; Konrad, M. *J. Mater. Chem.* **2003**, *13*, 2671.
(4) Magerle, R.; Krausch, G. *Adv. Mater.* **2002**, *14*, 1579.
(5) Jacob., N.; Israelachvli, D.; Michell, J.; Ninham, B. W. *J. Chem. Soc., Faraday Trans. 2* **1976**, *72*, 1525.
(6) Fasolka, M. J.; Mayes, A. M. *Annu. Rev. Mater. Res.* **2001**, *31*, 323.
(7) Riess, G. *Prog. Polym. Sci.* **2003**, *28*, 1107.
(8) Forster, S.; Zisenis, M.; Wenz, E.; Antonietti, M. *J. Chem. Phys.* **1996**, *104*, 9956.
(9) Peleshanko, S.; Tsukruk, V. V. *Prog. Polym. Sci.* **2008**, *33*, 523.
(10) Pitsikalis, M.; Pispas, S.; Mays, J. W.; Hadjichristidis, N. *Adv. Polym. Sci.* **1998**, *135*, 1.
(11) Hirao, A.; Hayashi, M.; Loykulnant, S.; Sugiyama, K.; Ryu, S. W.; Haraguchi, N.; Matsuo, A.; Higashihara, T. *Prog. Polym. Sci.* **2005**, *30*, 111.
(12) Hadjichristidis, N. *J. Polym. Sci., Part A: Polym. Chem.* **1999**, *37*, 857.
(13) Beyer, F. L.; Gido, S. P.; Poulos, Y.; Avgeropoulos, A.; Hadjichristidis, N. *Macromolecules* **1997**, *30*, 2373.
(14) Beyer, F.; Gido, S. P.; Uhrig, D.; Mays, J. W.; Tan, N. B.; Trevino, S. F. *J. Polym. Sci., Part B: Polym. Phys.* **1999**, *37*, 3392.
(15) Grayer, V.; Dormidontova, E.; Hadziioannou, G.; Tsitsilianis, C. *Macromolecules* **2000**, *33*, 6330.
(16) Stepanek, M.; Matejicek, P.; Humpolickova, J.; Havrankova, J.; Podhajecka, K.; Spirkova, M.; Tuzar, Z.; Tsitislianis, C.; Prochazka, K. *Polymer* **2005**, *46*, 10493.
(17) Tsitsilianis, C.; Chaumont, P.; Remmp, P. *Makromol, Chem.* **1990**, *191*, 2319.
(18) Tsitsilianis, C.; Voulgaris, D. *Macromol. Chem. Phys.* **1997**, *198*, 997.
(19) Kanaoka, S.; Omura, T.; Sawamoto, M.; Higashimura, T. *Macromolecules* **1992**, *25*, 6407.
(20) Tsitislianis, C.; Graff, S.; Rempp, P. *Eur. Polym. J.* **1991**, *27*, 243.
(21) Avgeropoulos, A.; Poulos, Y.; Hadjichristidis, N. *Macromolecules* **1996**, *29*, 6076.
(22) Voulgaris, D.; Tsitsilianis, C.; Esselink, F. J.; Hadziioannou, G. *Polymer* **1998**, *39*, 6429.
(23) Tsitsilianis, C.; Voulgaris, D. *Macromol. Reports* **1995**, *A32*, 569.
(24) Ge, Z.; Xu, J.; Wu, D.; Narain, R.; Liu, S. *Macromol. Chem. Phys.* **2008**, *209*, 754.
(25) Kyriazis, A.; Thierry, A.; Burchard, W.; Tsitsilianis, C. *Polymer* **2009**, *50*, 3204.
(26) (a) Peleshanko, S.; Gunawidjaja, R.; Jeong, J.; Shevchenko, V. V.; Tsukruk, V. V. *Langmuir* **2004**, *20*, 9423. (b) Peleshanko, S.; Jeong, J.; Gunawidjaja, R.; Tsukruk, V. V. *Macromolecules* **2004**, *37*, 6511. (c) Gunawidjaja, R.; Peleshanko, S.; Tsukruk, V. V. *Macromolecules* **2005**, *38*, 8765.
(27) Genson, K. L.; Hoffman, J.; Teng, J.; Zubarev, E. R.; Vaknin, D.; Tsukruk, V. V. *Langmuir* **2004**, *20*, 9044.
(28) Gunawidjaja, R.; Peleshanko, S.; Kirsten, L. G.; Tsitsilianis, C.; Tsukruk, V. V. *Langmuir* **2006**, *22*, 6168.
(29) Pispas, S.; Hadjichristidis, N.; Potemkin, I.; Khokhlov, A. *Macromolecules* **2000**, *33*, 1741.
(30) Lupitskyy, R.; Roiter, Y.; Tsitsilianis, C.; Minko, S. *Langmuir* **2005**, *21*, 8591.
(31) Gorodyska, G.; Kiriy, A.; Minko, S.; Tsitsilianis, C.; Stamm, M. *Nano Lett.* **2003**, *3*, 365.
(32) Kiriy, A.; Gorodyska, G.; Minko, S.; Stamm, M.; Tsitsilianis, C. *Macromolecules* **2003**, *36*, 8704.
(33) Yu, Y.; Chien, W.; Chen, S. *Polym. Int.* **2008**, *57*, 1369.
(34) Zhu, J.; Lennox, R. B.; Eisenberg, A. *Langmuir* **1991**, *7*, 1579.
(35) Zhu, J.; Eisenberg, A.; Lennox, R. B. *J. Am. Chem. Soc.* **1991**, *113*, 5583.
(36) Zhu, J.; Einsenberg, A.; Lennox, R. B. *Macromolecules* **1992**, *25*, 6556.
(37) Zhu, J.; Lennox, R. B.; Einsenberg, A. *J. Phys. Chem.* **1992**, *96*, 4727.
(38) Zhu, J.; Einsenberg, A.; Lennox, R. B. *Macromolecules* **1992**, *25*, 6547.
(39) Cox, J. K.; Yu, K.; Constantine, B.; Eisenberg, A.; Lennox, R. B. *Langmuir* **1999**, *15*, 7717.
(40) Francis, R.; Skolnik, A. M.; Carino, S. R.; Logan, J. L.; Underhill, R. S.; Angot, S.; Taton, D.; Gnanon, Y.; Duran, R. S. *Macromolecules* **2002**, *35*, 6483.
(41) Logan, J. L.; Masse, P.; Gnanou, Y.; Taton, D.; Duran, R. *Langmuir* **2005**, *21*, 7380.
(42) Joncheray, T. J.; Denoncourt, K. M.; Mathieu, C.; Meier, M. A. R.; Schubert, U. S.; Duran, R. S. *Langmuir* **2006**, *22*, 9264.
(43) Hammond, M. R.; Li, C.; Tsitsilianis, C.; Mezzenga, R. *Soft Matter* **2009**, *5*, 2371.
(44) Zheng, W.; Wang, Z. *Macromolecules* **1995**, *28*, 7215.
(45) Hadjichristidis, N.; Iatrou, H.; Pitsikalis, M.; Pispas, S.; Avgeropoulos, A. *Prog. Polym. Sci.* **2005**, *30*, 725.
(46) Zhang, L; Eisenberg, A. *J. Am. Chem. Soc.* **1996**, *118*, 3169.
(47) Discher, D. E.; Eisenberg, A. *Science* **2002**, *297*, 967.
(48) Li, Z.; Kesselman, E.; Talmon, Y.; Hillmyer, M. A.; Lodge, T. P. *Science* **2004**, *206*, 98.
(49) Pochan, D. J.; Chen, Z.; Cui, H.; Hales, K.; Qi, K.; Wooley, K. L. *Science* **2004**, *306*, 94.
(50) Cornelissen, J.; Fischer, M.; Sommerdijk, N.; Nolte, R. J. M. *Science* **1998**, *280*, 1427.
(51) Fustin, C. A.; Abetz, V.; Gohy, J. F. *Eur. Phys. J.* **2005**, *E16*, 291.
(52) (a) Szunerits, S.; Boukherroub, R. *Langmuir* **2006**, *22*, 1660. (b) Sheller, N. B.; Petrash, S.; Foster, M. D.; Tsukruk, V. V. *Langmuir* **1998**, *14*, 4535.
(53) (a) Larson, K.; Vaknin, D.; Villavicencio, O.; McGrath, D. V.; Tsukruk, V. V. *J. Phys. Chem. B* **2002**, *106*, 7246. (b) Peleshanko, S.; Sidorenko, A.; Larson, K.; Villavicencio, O.; Ornatska, M.; McGrath, D. V.; Tsukruk, V. V. *Thin Solid Films* **2002**, *406*, 233.
(54) Ulman, A. *An Introduction to Ultrathin Organic Films: From Langmuir-Blodgett to Self-Assembly*; Academic Press: Boston, MA, 1991.
(55) (a) Tsukruk, V. V.; Reneker, D. H. *Polymer* **1995**, *36*, 1791. (b) Tsukruk, V. V. *Rubber Chem. Technol.* **1997**, *70*, 430.
(56) Magonov, S. N.; Elings, V.; Whangbo, M. H. *Surf. Sci.* **1997**, *375*, L385.
(57) Kim, B.-S.; Gao, H.; Argun, A. A.; Matyjaszewski, K.; Hammond, P. T. *Macromolecules* **2009**, *42*, 368.
(58) Li, S.; Clarke, C. J.; Eisenberg, A.; Lennox, R. B. *Thin Solid Films* **1999**, *354*, 136.
(59) Shin, K.; Rafailovich, M. H.; Sokolov, J.; Chang, D. M.; Cox, J. K.; Lennox, R. B.; Eisenberg, A.; Gibaud, A.; Huang, J.; Hsu, S. L.; Satija, S. K. *Langmuir* **2001**, *17*, 4955.
(60) Wen, G.; Chung, B.; Chang, T. *Polymer* **2006**, *47*, 8575.
(61) Goncalves da Silva, A. M.; Filipe, E. J. M.; dOliveira, J. M. R.; Martinho, J. M. G. *Langmuir* **1996**, *12*, 6547.
(62) Chung, B.; Choi, M.; Ree, M.; Jung, J. C.; Zin, W. C.; Chang, T. *Macromolecules* **2006**, *39*, 684.
(63) Voulgaris, D.; Tsitsilianis, C.; Grayer, V.; Esselink, F. J.; Hadziioannou, G. *Polymer* **1999**, *40*, 5879.